

MOF-derived Co₃O₄/Nitrogen-doped Carbon Composite for Chlorine-assisted Production of Ethylene Oxide

Tianlei Li^a, Hengzhou Liu^a, Jiaqi Yu^b, Yifu Chen^a, Wenyu Huang^b, and Wenzhen Li^{a*}

Corresponding author: wzli@iastate.edu

- a. Department of Chemical and Biological Engineering, Iowa State University, Ames, Iowa 50011, United States
- b. Department of Chemistry, Iowa State University, Ames, Iowa 50011, United States

*Corresponding author: wzli@iastate.edu

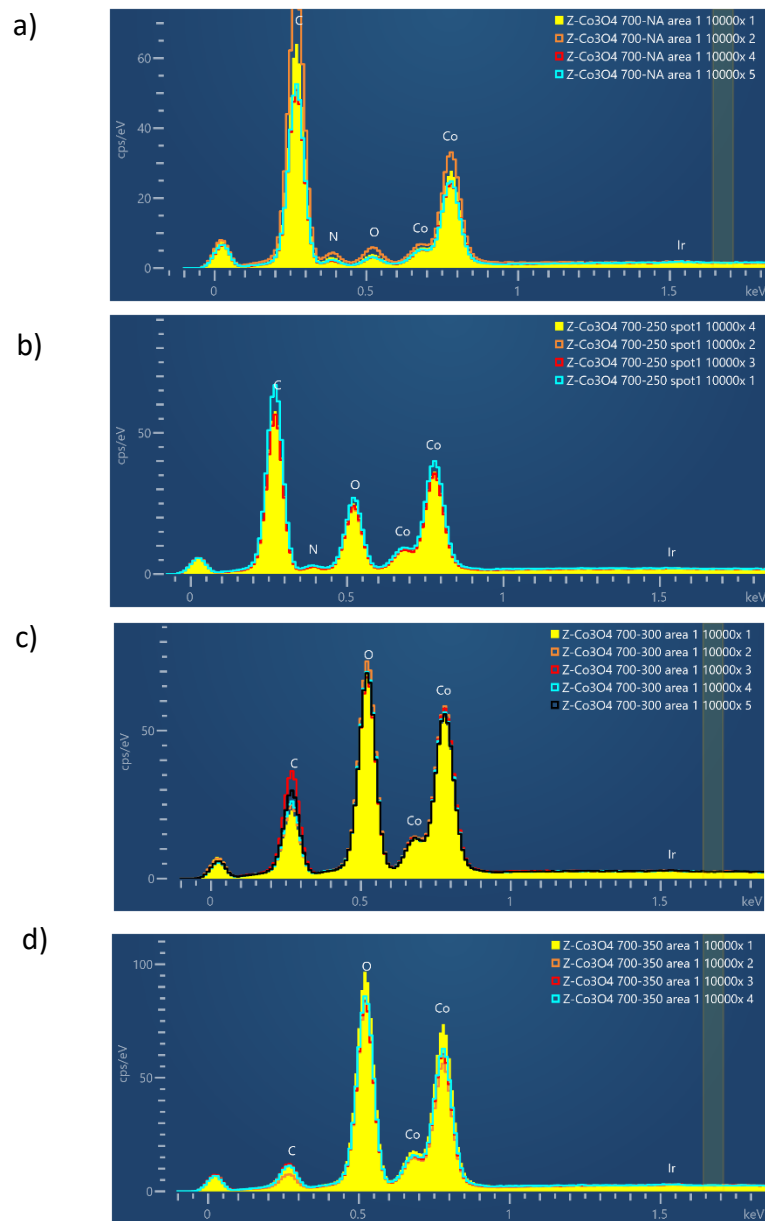


Figure S1. EDS spectra of **a)** ZCO-700-NA, **b)** ZCO-700-250, **c)** ZCO-700-300, **d)** ZCO-700-350. 4 or 5 sets of EDS data were taken from different sites on one sample to minimize the possible error because EDS could only show the signal from a small surface area. Higher O: Co ration with rising temperature was observed.

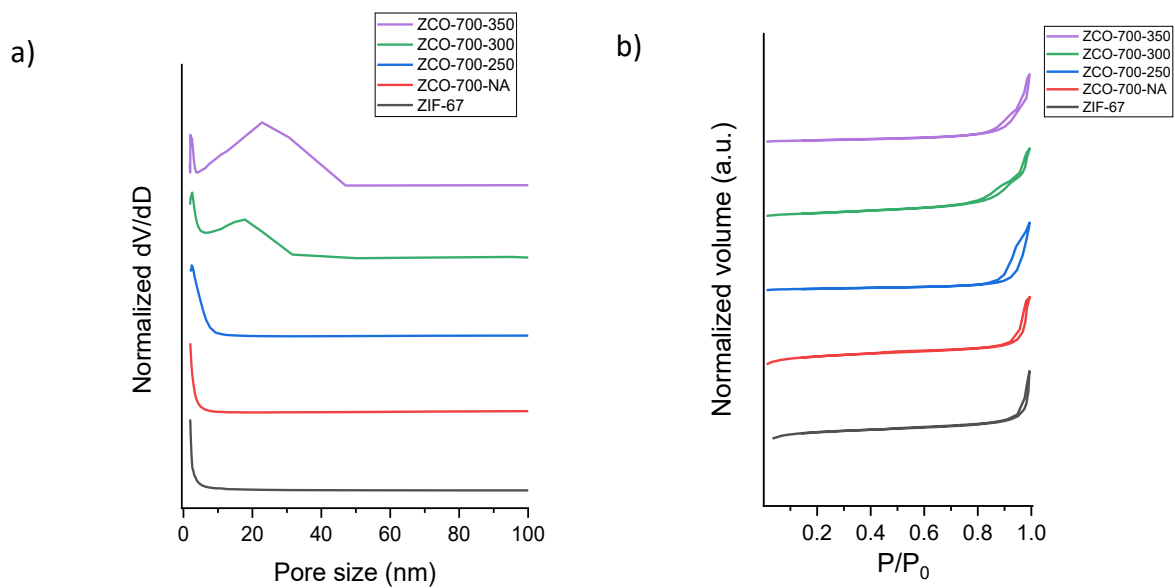


Figure S2. a) pore size distribution. **b)** BET plot. In a), large pores formed and took a higher portion as temperature elevated. In b), all samples showed a type IV loop, which indicated the porous structure of the samples.

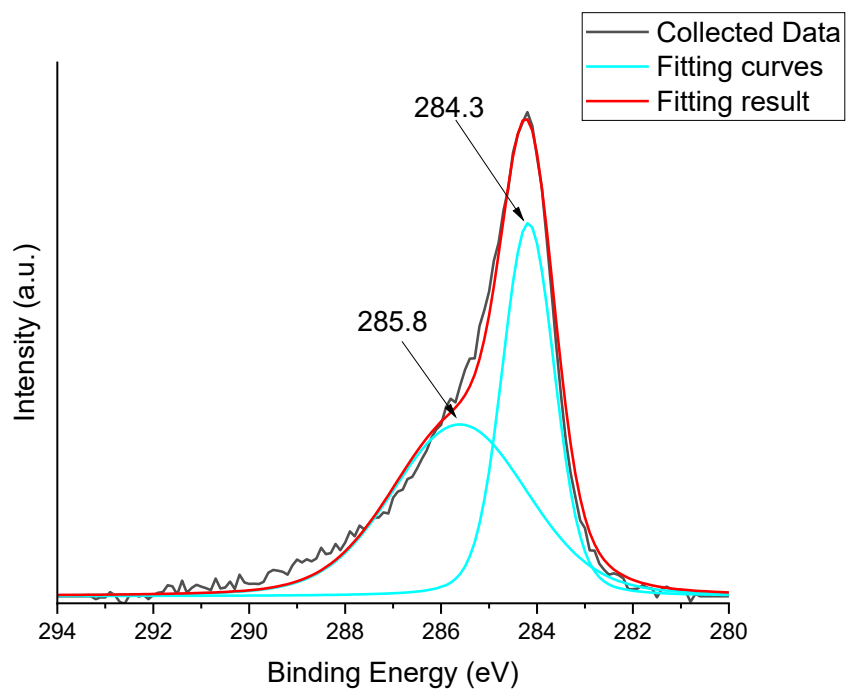


Figure S3 XPS fitting curve for C 1s orbital of ZCO-700-300. The peak at 284.3 eV was assigned to C-C and C=C bonds. The peak at 285.8 eV was associated with C-N bond¹, which proved that carbon content was doped with nitrogen.

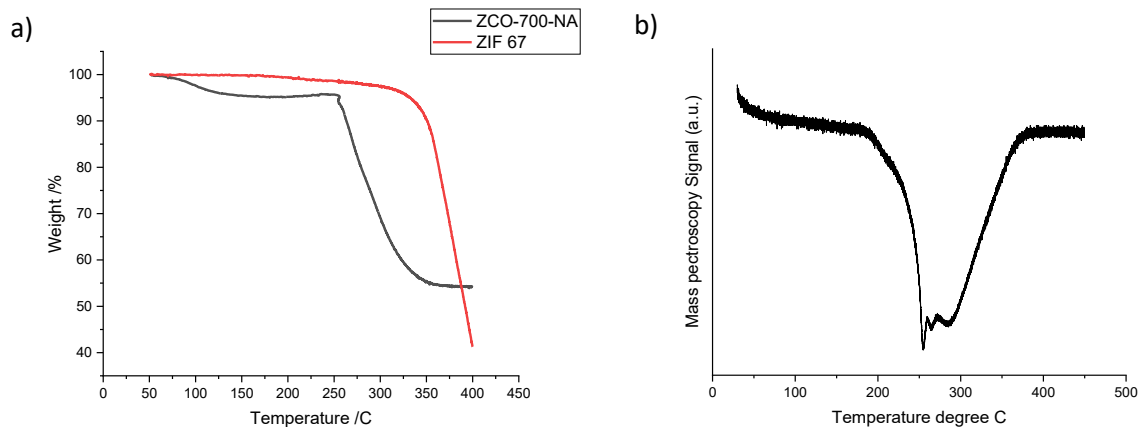


Figure S4. a) TGA result of ZIF-67 and ZCO-700-NA. **b)** TPO results of oxygen absorption on ZCO-700-NA. Three adsorption peaks were observed in TPO results at 250, 270 and 290 °C respectively. The first peak was assigned to the metallic Co that was not in the framework. This is the reason for some Co_3O_4 presence in ZCO-700-250. A longer calcination time was tested, but nothing changed in the electrochemical test. This indicated that there were two kinds of Co. One could be oxidized at a lower temperature, and one needs a higher temperature to be oxidized. The second adsorption peak was associated with carbon oxidation because the sample was still a mixture of Co and Co_3O_4 . The third peak was assigned to the rest of the Co oxidation as a pure Co_3O_4 XRD pattern was observed at ZCO-700-300.

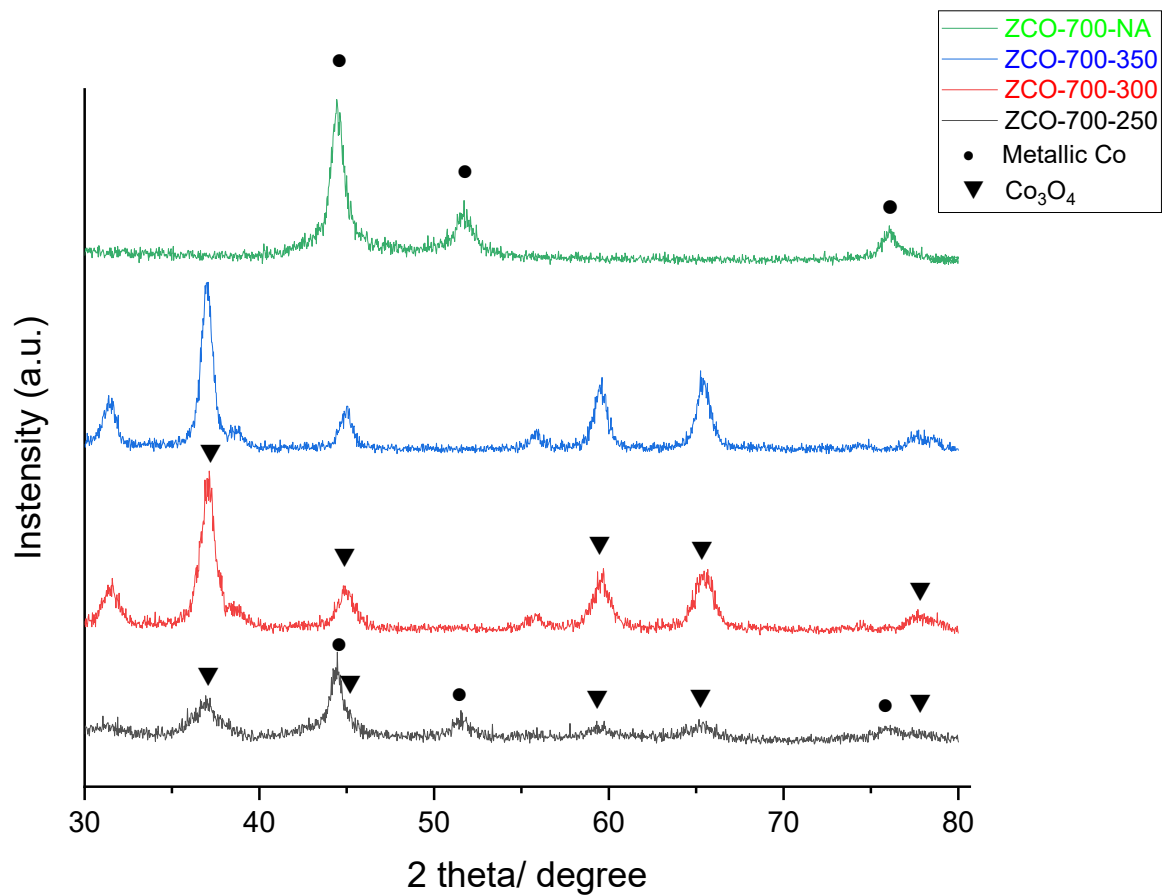


Figure S5. XRD data for samples made through two-step calcination. It was obvious that ZCO-700-250 contains peaks of both Co and Co₃O₄, which supported that Co was not fully oxidized at 250 °C.

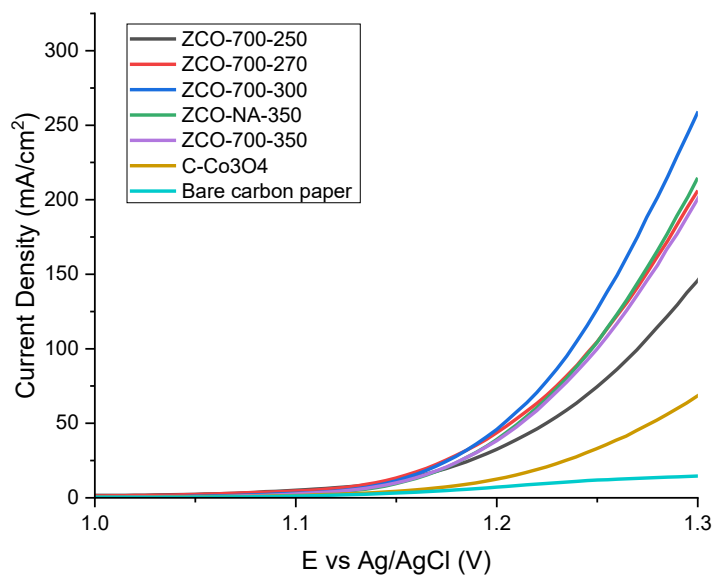


Figure S6. LSV comparison between samples prepared at different temperatures. ZCO-700-300 showed best activity in all prepared samples.

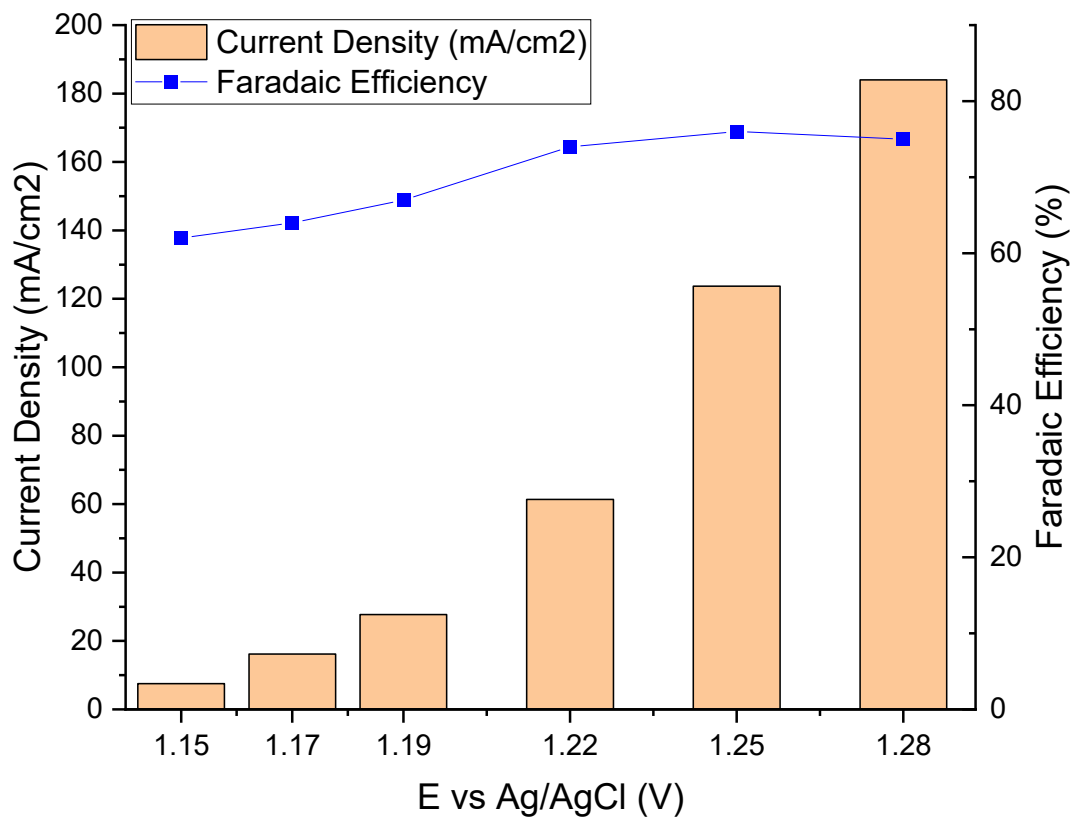


Figure S7. Current and faradaic efficiency dependence on potential.

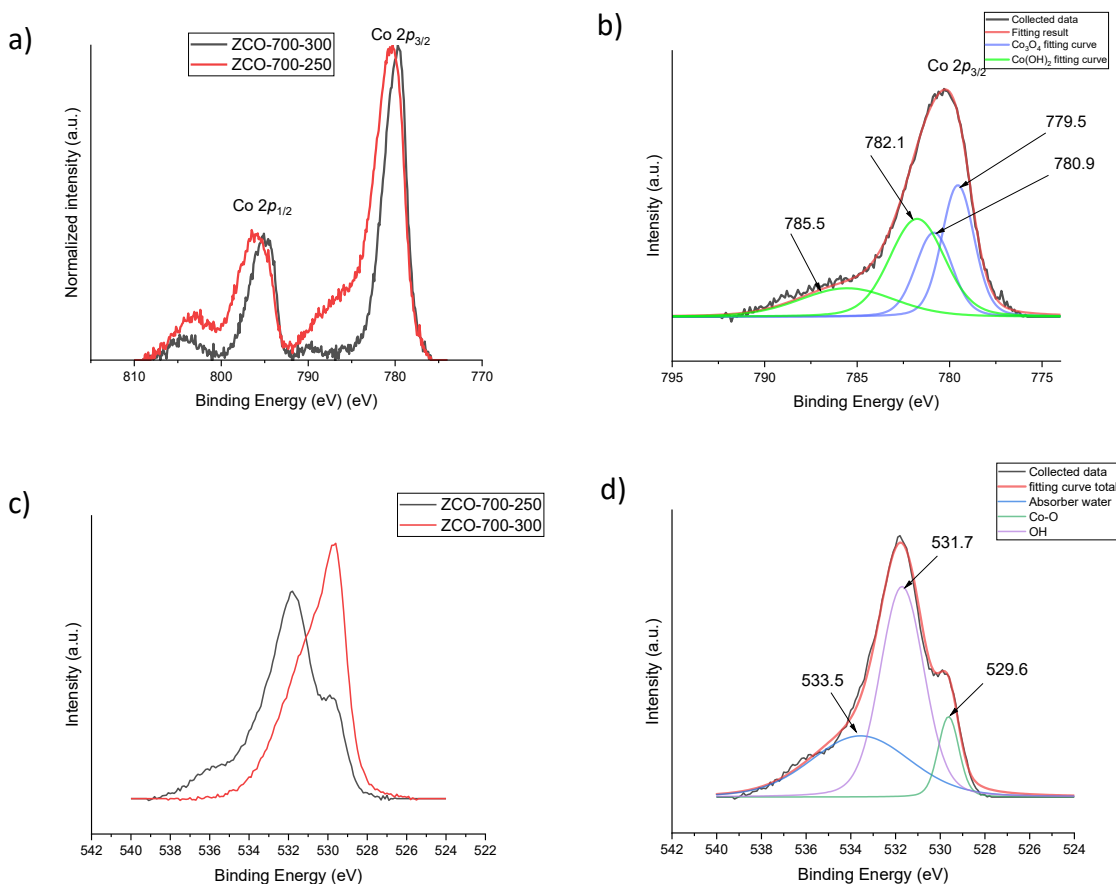


Figure S8. XPS of **a) Co 2p**, **b) peak fitted Co $2p_{3/2}$** spectrum for ZCO-700-250 after electrolysis **c) O 1s** after electrolysis **d) peak fitted O 1s** spectrum for ZCO-700-250 after electrolysis. In a), the little left shift of the ZCO-700-250 Co $2p_{3/2}$ peak and a satellite peak at 786.3 eV are evidence of the presence of Co(OH)₂. In b), peak fitting was performed for ZCO-700-250 Co $2p_{3/2}$ spectrum, which fits the peaks with Co(OH)₂ and Co₃O₄ mixture very well. The peaks at 779.5, 781.0, and 782.1 eV could be assigned to Co³⁺, Co²⁺ in Co₃O₄, and Co²⁺ in Co(OH)₂, respectively. The distinct peak at 785.5 eV was assigned to satellite peak, which was unique for Co(OH)₂. To further confirm the species, O 1s spectrum was also examined. In c), it compares O 1s spectra between ZCO-700-250 and ZCO-700-300. There was a distinctive peak difference. In d) it showed the peak fitting of O 1s of ZCO-700-250. The peaks at 529.6, 531.7 and 533.5 eV are assigned to oxygen connected to cobalt, OH group and absorbed water on the sample, which further supported the presence of Co(OH)₂. Co(OH)₂ has been reported to show remarkable OER activity.

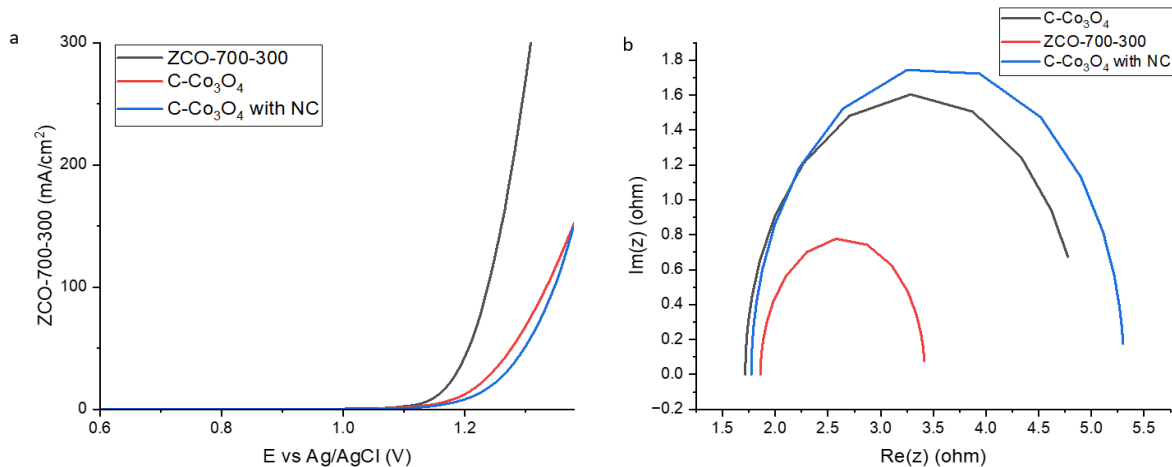


Figure S9 a) LSV b) EIS comparison with ZCO-700-300, C-Co₃O₄ and C-Co₃O₄ with NC. We believe C-Co₃O₄-NC does not form any heterojunction because its preparation is merely through physical mixing of Co₃O₄ and NC. Therefore, C-Co₃O₄-NC can be used to compare to our MOF-derived sample with possible formation of heterojunction. As shown in this figure, the charge transfer resistance and total activity performance of C-Co₃O₄-NC is very similar to that of C-Co₃O₄. By comparing their specific activity, the ZCO-700-300 is about 50% greater than C-Co₃O₄-NC and C-Co₃O₄. Since the Co₃O₄ in ZCO-700-300 has been oxidized by heating in air. We do not believe there is any difference in terms of crystal structure compared to commercial Co₃O₄. Therefore, we can logically assume the better activity could be due to the formation of heterojunction or better surface utilization.

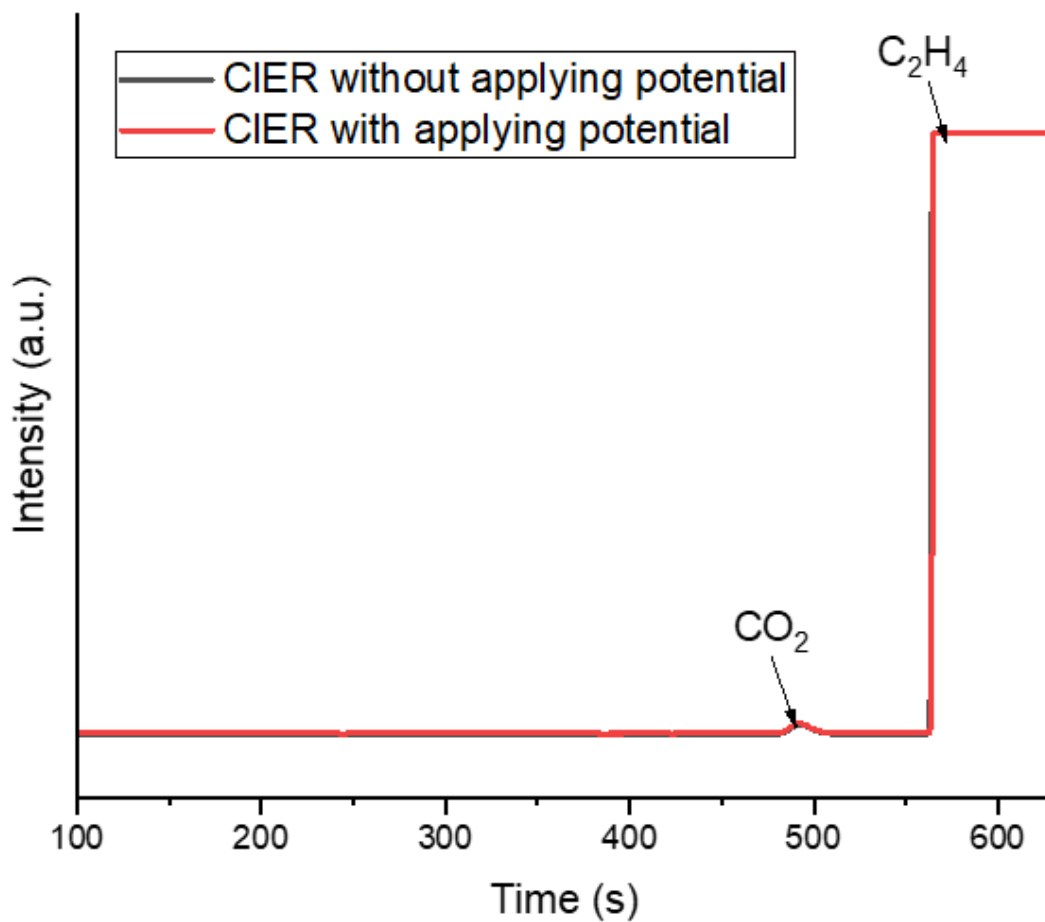


Figure S10, online GC result of CIER. It should be noted that the possible products other than oxygen and chloroethanol or ethylene oxide can be some other partial C_2H_4 oxidation products or total oxidation to CO_2 . No signals other than CO_2 and C_2H_4 was observed from the FID detector, as shown in this figure. CO_2 concentration was similar to the blank test, which means there is no or trace amount of C_2H_4 was oxidized to CO_2 .

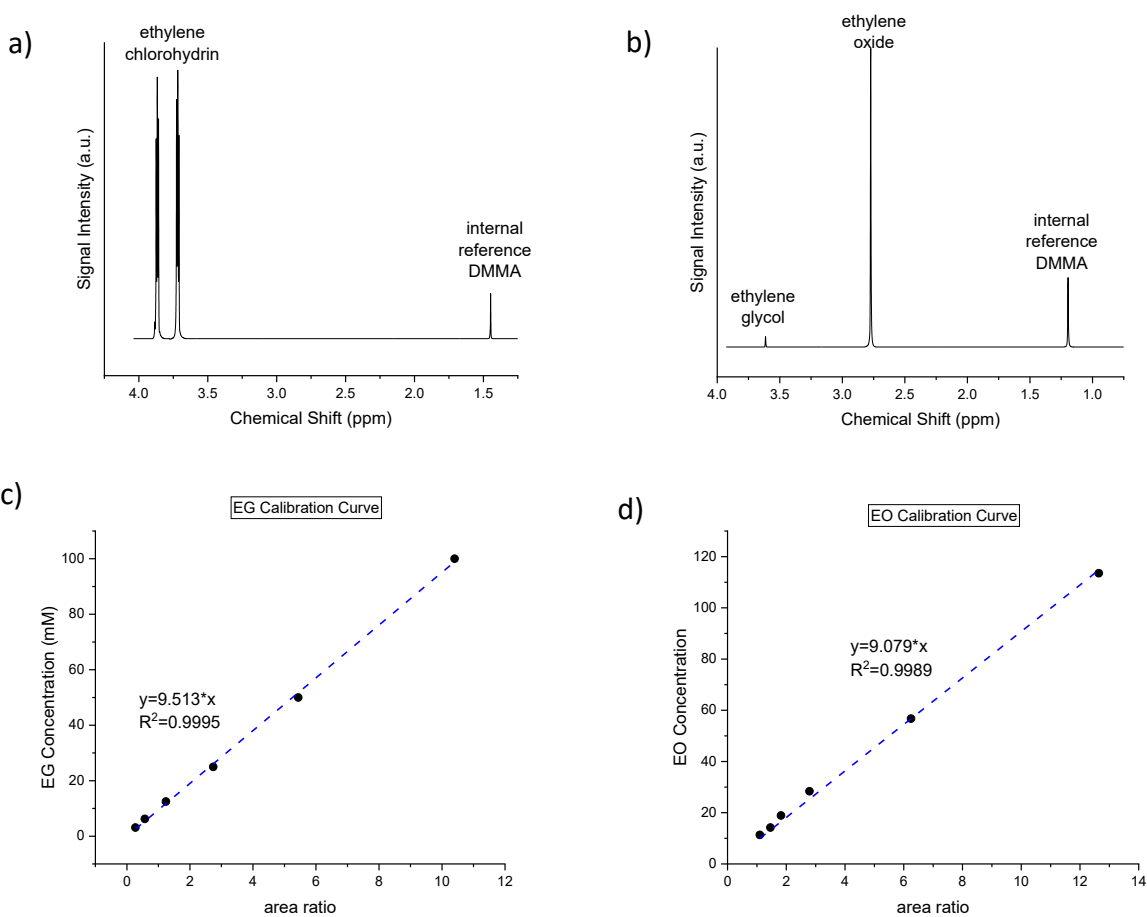


Figure S11, NMR results **a)** Example of 2-chloroethanol **b)** example of mixing 2-chloroethanol with catholyte and forming ethylene oxide and ethylene glycol. Ethylene glycol took up about 3% of the whole product. **c)** calibration curve of known concentration of ethylene glycol with respect to area ratio between product and internal reference. **d)** calibration curve of known concentration of ethylene oxide with respect to area ratio between product and internal reference. The internal reference peak shift is due to different aqueous environments. The calibration curve intercept was set to 0.

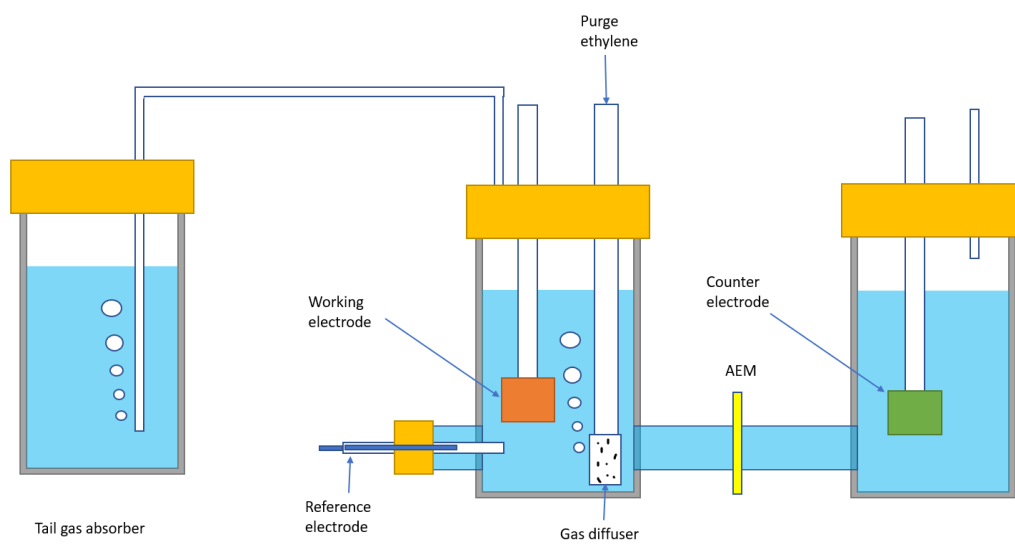


Figure S12. Schematic of the H-cell setup with tail gas absorber

Table S1. Surface area measured by nitrogen physisorption, and equivalent active content measured by TGA.

Sample name	BET surface area (m ² /g)	Active content/ wt%
ZIF 67	1304.96	41
ZCO-700-NA	310.08	54
ZCO-700-250	203.35	59
ZCO-700-300	106.90	86
ZCO-700-350	65.75	98
ZCO-NA-350	54.73	99
ZCO-NA-400	36.55	100
Commercial Nano Co ₃ O ₄	17.48	100

Table S2. Performance comparison with cited works.

Material	Equivalent Loading (mg/cm ²)	Electrolyte Concentration (M)	Potential (V vs SHE) ¹	Current Density (mA/cm ²)	Faradaic Efficiency (%)	Ref
Co ₃ O ₄	1	2	1.427	100	82	This work
IrO ₂ -Co ₃ O ₄	0.96 (Co ₃ O ₄) + 1.13 (IrO ₂)	2	1.637	100	99	[1] ²
		0.01	1.887	10	38	
Pt-CNT	0.1	1	1.366	50	N/A	[2]
		0.1	1.475	10	96	
IrO ₂	1	2	2.8	300	71	[3] ²
CoSb ₂ O _x	0.096 (Co) + 0.023 (Sb)	4	1.833	100	96	[4]
Co ₃ O ₄	0.86	0.6	1.4	10	82	[5]
Co ₃ O ₄	1.5	0.6	1.6	62	55	[6] ³
Co ₃ O ₄	0.6	0.5	1.564	20	82	[7]
Co ₃ O ₄	0.7	5	1.778	100	86	[8] ⁴

Notes:

- 1) Potentials were converted to SHE based on reported conditions
- 2) Results were not IR corrected
- 3) Experiment was carried out at pH=8 buffered solution
- 4) Experiment was carried out at pH=3 buffered solution

Reference

1. Xing, Z.; Ju, Z.; Zhao, Y.; Wan, J.; Zhu, Y.; Qiang, Y.; Qian, Y., One-pot hydrothermal synthesis of Nitrogen-doped graphene as high-performance anode materials for lithium ion batteries. *Sci Rep* **2016**, *6*, 26146.
2. Han, S.; Kim, S.; Kwak, S.; Lee, C.; Hong Jeong, D.; Kim, C.; Yoon, J., Iridium-cobalt mixed oxide electrode for efficient chlorine evolution in dilute chloride solutions. *Journal of Industrial and Engineering Chemistry* **2022**, *108*, 514-521.
3. Lim, T.; Kim, J. H.; Kim, J.; Baek, D. S.; Shin, T. J.; Jeong, H. Y.; Lee, K.-S.; Exner, K. S.; Joo, S. H., General Efficacy of Atomically Dispersed Pt Catalysts for the Chlorine Evolution Reaction: Potential-Dependent Switching of the Kinetics and Mechanism. *ACS Catalysis* **2021**, *11* (19), 12232-12246.
4. Leow Wan, R.; Lum, Y.; Ozden, A.; Wang, Y.; Nam, D.-H.; Chen, B.; Wicks, J.; Zhuang, T.-T.; Li, F.; Sinton, D.; Sargent Edward, H., Chloride-mediated selective electrosynthesis of ethylene and propylene oxides at high current density. *Science* **2020**, *368* (6496), 1228-1233.
5. Moreno-Hernandez, I. A.; Brunshwig, B. S.; Lewis, N. S., Crystalline nickel, cobalt, and manganese antimonates as electrocatalysts for the chlorine evolution reaction. *Energy & Environmental Science* **2019**, *12* (4), 1241-1248.
6. Ha, H.; Jin, K.; Park, S.; Lee, K.-G.; Cho, K. H.; Seo, H.; Ahn, H.-Y.; Lee, Y. H.; Nam, K. T., Highly Selective Active Chlorine Generation Electrocatalyzed by Co₃O₄ Nanoparticles: Mechanistic Investigation through in Situ Electrokinetic and Spectroscopic Analyses. *The Journal of Physical Chemistry Letters* **2019**, *10* (6), 1226-1233.
7. Chung, M.; Jin, K.; Zeng, J. S.; Manthiram, K., Mechanism of Chlorine-Mediated Electrochemical Ethylene Oxidation in Saline Water. *ACS Catalysis* **2020**, *10* (23), 14015-14023.
8. Wang, H.; Li, J.; Zhang, D.; Wang, G.; Wang, P., Morphology regulation and application of nano cobalt oxide (Co₃O₄) electrocatalysts for chlorine evolution toward marine anti-biofouling. *Journal of Colloid and Interface Science* **2022**, *628*, 794-806.
9. Zhu, X.; Wang, P.; Wang, Z.; Liu, Y.; Zheng, Z.; Zhang, Q.; Zhang, X.; Dai, Y.; Whangbo, M.-H.; Huang, B., Co₃O₄ nanobelt arrays assembled with ultrathin nanosheets as highly efficient and stable electrocatalysts for the chlorine evolution reaction. *Journal of Materials Chemistry A* **2018**, *6* (26), 12718-12723.